2013

Assessing tumor physiology by dynamic contrast-enhanced near-infrared spectroscopy

Kyle Verdecchia
Western University

Jonathan Elliott
Western University

Mamadou Diop
Western University

Lisa Hoffman
Western University

Ting-Yim Lee
Western University

See next page for additional authors

Authors
Kyle Verdecchia, Jonathan Elliott, Mamadou Diop, Lisa Hoffman, Ting-Yim Lee, and Keith St. Lawrence

PROCEEDINGS OF SPIE

SPIEDigitalLibrary.org/conference-proceedings-of-spie

Assessing tumor physiology by dynamic contrast-enhanced near-infrared spectroscopy

Kyle Verdecchia
Jonathan Elliott
Mamadou Diop
Lisa Hoffman
Ting-Yim Lee
Keith St. Lawrence

SPIE.

Assessing tumor physiology by dynamic contrast-enhanced near-infrared spectroscopy

Kyle Verdecchia*[a,b], Jonathan Elliott[a,b], Mamadou Diop[a,b], Lisa Hoffman[a,b], Ting-Yim Lee[a,b,c], Keith St. Lawrence[a,b]

[a]Imaging Division, Lawson Health Research Institute, 268 Grosvenor Street, London, ON, Canada N6A 4V2; [b]Dept. of Medical Biophysics, Western University, 1151 Richmond Street, London, ON Canada N6A 3K7; [c]Imaging Program, Robarts Research Institute, 100 Perth Drive, London, ON Canada N6A 5K8

ABSTRACT

The purpose of this study was to develop a dynamic contrast-enhanced (DCE) near-infrared spectroscopy (NIRS) technique to characterize tumor physiology. Dynamic data were acquired using two contrast agents of different molecular weights, indocyanine green (ICG) and IRDye 800CW carboxylate (IRD_{cxb}). The DCE curves were analyzed using a kinetic model capable of extracting estimates of tumor blood flow (F), capillary transit time (t_c) and the amount of dye that leaked into the extravascular space (EVS) – characterized by the extraction fraction (E). Data were acquired from five nude rats with tumor xenografts (>10mm) implanted in the neck. Four DCE-NIR datasets (two from each contrast agent) were acquired for each rat. The dye concentration curve in arterial blood, which is required to quantify the model parameters, was measured non-invasively by dye densitometry. A modification to the kinetic model to characterize t_c as a distribution of possible values, rather than finite, improved the fit of acquired tumor concentration curves, resulting in more reliable estimates. This modified kinetic model identified a difference between the extracted fraction of IRD_{cxb}, 15 ± 6 %, and ICG, 1.6 ± 0.6 %, in the tumor, which can be explained by the difference in molecular weight: 67 kDa for ICG since it binds to albumin and 1.17 kDa for IRD. This study demonstrates the ability of DCE-NIRS to quantify tumor physiology. The next step is to adapt this approach with a dual-receptor approach.

Keywords: Dynamic-contrast enhanced, near-infrared spectroscopy, time-resolved, tumor, hemodynamics, adiabatic approximation to the tissue homogeneity

1. INTRODUCTION

Increased angiogenesis, the physiological process of generating new blood vessels, is a characteristic of cancer. Furthermore, because of the rapid growth of tumor vessels, they are often leaky compared to healthy tissue, and this can be detected by dynamic contrast-enhanced (DCE) imaging methods, including magnetic resonance imaging (MRI)[1] and computed tomography (CT)[2]. The methodology involves injecting a contrast agent into the blood system and using serial imaging to monitoring the uptake and clearance of the contrast agent. With MRI and CT, DCE imaging has become standard practice for assessing tumor hemodynamic properties in order to improve detection and grading of cancer. However, only few studies have applied DCE to optical methods[3,4], despite the potential advantages that optics provides in terms of safety, expense, and repeatability[5].

Our group has previously developed DCE near-infrared spectroscopy (NIRS) for assessing cerebral hemodynamics by using the optical contrast agent, indocyanine green (ICG)[6–8]. Because the blood-brain barrier remains intact in this application, cerebral blood flow, blood volume, and mean transit time are determined by a model-independent deconvolution approach. However, it is expected in tumors that contrast agents will leak out of the vasculature due to the poorly developed vessels[9]. To account for this feature, the deconvolution was performed using a model-based approach that explicitly describes both blood flow and vascular permeability. A variation of the tracer kinetic model that accounts for a distribution of tc values due to flow heterogeneity in tumors was also investigated. The purpose of this study was to assess the ability of these models to properly characterize DCE data acquired by time-resolved (TR)-NIRS. Experiments were conducted using human colon cancer xenographs grown subcutaneously in rats. Two contrast agents with different molecular-weights, ICG and IRDye 800CW carboxylate (IRD_{cbx}, LI-COR Biosciences), were used.

Optical Tomography and Spectroscopy of Tissue X, edited by Bruce J. Tromberg, Arjun G. Yodh, Eva Marie Sevick-Muraca, Proc. of SPIE Vol. 8578, 857823
 · doi: 10.1117/12.2004774

1.1 Tracer kinetic model

In all kinetic models, the concentration of the contrast agent within the interrogated tissue volume, for instance in a tumor, can be modeled as a linear time-invariant system, given by the convolution equation:

$$Q(t) = F \bullet C_a(t) * R(t) \tag{1}$$

where * is the convolution operator, Q(t) is the amount of contrast agent within the tumor, F is blood flow, and $C_a(t)$ is the time-varying contrast agent concentration in arterial blood. The function R(t) is referred to as the impulse residue function and it describes the amount of contrast agent remaining in the tumor following an idealized bolus injection at t equal to 0. R(t) is defined by the specific kinetic models which are described below.

1.2 Adiabatic approximation to the tissue homogeneity model

Multiple tracer kinetic models have been proposed for describing R(t). For this application, we selected the adiabatic approximation to the tissue homogeneity (AATH) model [10] because it accounts for a finite vascular transit time – unlike compartmental models that assume it is negligible are due to instantaneous mixing – and the exchange of contrast agent between blood and surrounding tissue. For the AATH model, R(t) is defined as follows:

$$R(t) = \begin{matrix} 1 & t < t_c \\ E \bullet e^{-k_e(t-t_c)} & t \geq t_c \end{matrix} \tag{2}$$

In Equation (2), the main components defined by the model are the capillary transit time, t_c, and the fraction of contrast agent extracted into the surrounding extravascular space during a single capillary transit, E. Also, the clearance rate of extracted contrast agent from the tumor is governed by the rate constant k_e. A caveat to the AATH model is transit through the tumor vasculature is defined by a single capillary transit time. This is likely an oversimplification when the model is applied to DCE data acquired from a large tissue volume.

1.3 Vascular dispersion model

A modification to the AATH model to account for the possibility of a distribution of t_c values has been proposed[11]. In this modification, referred to as the vascular dispersion (VD) model, the t_c distribution is modeled as gamma distribution:

$$R(t) = 1 - \int_0^t g(u)du + E \bullet e^{-k_e t} \int_0^t g(u) e^{k_e u} du \tag{3}$$

where the addition function, g(t), refers to the gamma distribution:

$$g(t) = \frac{t^{\alpha-1} e^{t/\tau}}{\tau^{\alpha} \int_0^{\infty} t^{\alpha-1} e^{-t} dt}, \; for \tau \geq 0 \tag{4}$$

and $\tau = t_c/\alpha$. Compared to the AATH model, a new parameter, α, is introduced to characterize the width of vascular dispersion ($0 \leq \alpha^{-1} \leq 1$).

2. METHODS

2.1 Time-resolved near-infrared spectroscopy system

A time-resolved NIRS system consisting of picosecond pulsed diode laser (LDH-P-C-810, PicoQuant, Germany) was used to acquire the DCE data[8]. The wavelength of the emitted light by the laser was 802 nm with an output power and pulse repetition rate of 1.4 mW and 80 MHz, respectively. The laser beam was coupled into a 1.5-m long multimode fiber (N.A. = 0.22, core = 400 μm, Fiberoptics Technology, Pomfret, Connecticut) and attenuated by two variable neutral density filters (NDC-50-4M, Thorlabs, Newton, NJ) before transmitting through tissue. The diffuse light was

detected by a 2-m fiber optic bundle (N.A. = 0.55, 3.6 mm active area and 4.7 mm outer diameter; Fiberoptics Technology) coupled to a Peltier-cooled photomultiplier tube (PMC-100, Becker & Hickl, DE). Detection of single photons generated electrical pulses (amplitude = 50-200 mV, width = 1.5 ns) that were transmitted to a time-correlated single photon counting (TCSPC) module (SPC-134, Becker & Hickl, Germany). Before tissue data were acquired, the instrument response function (IRF) was measured at the start of each experiment to account for light dispersion by the TR-NIRS system[12].

2.2 Rat model

All experimental procedures were approved by the Animal Use Subcommittee of the University of Western Ontario. The LoVo human colon adenocarcinoma cell line (no. CCL-229; ATCC, Manassas, VA) was maintained in F12K growth medium (Gibco, Burlington, Ontario, Canada), supplemented with 10% fetal bovine serum. Cells were implanted onto the neck of male T-cell deficient athymic nude rats (Crl:NIH-rnu, Charles River Laboratories,Wilmington,MA) between the ages of four to six weeks old. For implantation, the cells were suspended at a concentration of 108 cells/ml in serum-free F12K medium with penicillin (100 U/ml) and streptomycin (100 µl/ml) added before 150 microliters of the cell suspension (1.5×10^7 cells/rat) were implanted subcutaneously. Experiments were conducted approximately two weeks after implantation when tumors had reached a minimal diameter of 10 mm.

2.3 Experimental setup

Rats were anaesthetized by inhaling 4% isoflurane before inserting a catheter into a tail vein, which was used to collect blood samples and to inject contrast agents. The emission and detection optical fibers were placed transversely onto the tumor surface using in-house developed probe holders. The diameter of each tumor was measured by callipers. Four sets of DCE data were collected per rat and each set contained a total acquisition time of 5 minutes. Successive injection of contrast agents was separated by roughly 30 minutes to allow contrast agent clearance from the previous injection. The first two injections were ICG due to its faster clearance, followed by the two IRD_{cxb} injections. The contrast agents were intravenously injected as a bolus at a concentration of 0.7 mg/kg dissolved in 0.5 ml sterile water. Serial tissue tracer concentration measurements were made every 0.4 s for 15 s prior to and 5 min following injection of the contrast agent. The arterial input function (AIF) was measured concurrently by a dye densitometer attached to a rear foot (DDG 2001, Nihon Kohden, Japan).

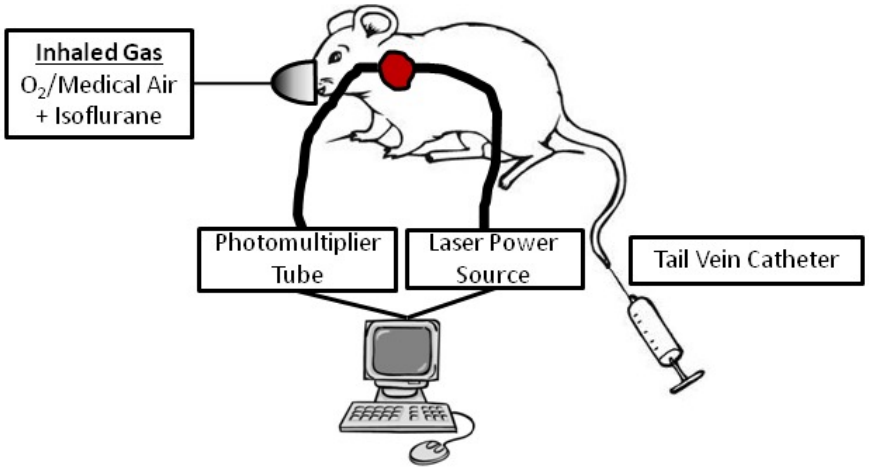

Figure 1. A schematic diagram of the experimental setup

2.4 Data Analysis

Quantification of tumor optical properties was performed by fitting the solution to the diffusion equation for transmittance through an infinite homogenous slab[13]. For each injection, the concentration of contrast agent in the tumor, Q(t), was determined in two steps. First, the baseline optical properties (the absorption coefficient, μ_a, and the reduced scattering coefficient, μ_s') were determined from temporal point spread functions (TPSFs) acquired for 30 seconds before injecting a contrast agent. Second, the time-varying change in μ_a caused by the injected contrast agent was determined by analyzing each TPSF in the time series by fitting for μ_a and setting μ_s' to its baseline value. Using

the known extinction coefficient of the active contrast agent at 802 nm, the time-dependent change in $\mu_a(t)$ was converted into concentration. Simultaneously, data obtained by the dye densitometer were converted into the arterial contrast agent concentration, $C_a(t)$, by using the measured total hemoglobin blood concentration (tHb) for each rat and the molecular weight of the contrast agent.

The kinetic models were fit to the DCE data by nonlinear optimization (MATLAB® function fminsearch). The fitting parameters were F, t_c, E, and k_e for both models. The VD model also included the additional fitting parameter α to account for the distribution of capillary transit times. All parameters were constrained to be positive, the upper limit of both E and α^{-1} was set to 1. To account for differences in the arrival time of contrast agent between tissue and arterial blood, the fitting was repeated while shifting the arterial data by the sampling interval (0.4 s). The optimal time shift was selected based on the minimum sum of squared differences between the data and the model. From the best-fit estimates of the model parameters, tumor blood volume (V_c) was determined using the central volume principle, $V_c = F \cdot t_c$ and the permeability surface-area (PS) product was determined from $E = 1\text{-}e^{-PS/F}$.

3. RESULTS AND DISCUSSION

3.1 Physiological Parameters

A total of 5 rats were used in this study and all errors are given as standard error. Table 1 contains the individual physiological parameters for each individual rat. The average values were 310 ± 20 g for weight, 13 ± 4 mm for tumor diameter, 95 ± 3 % for arterial oxygen saturation (SO_2), 360 ± 30 beats per minute (BPM) for heart rate, and 12.7 ± 1.0 g/dl for tHb.

Table 1. Physiological parameters for each rat within the study.

Rat	Weight (g)	Diameter (mm)	SO_2 (%)	Heart Rate (BPM)	tHb (g/dl)
1	286	12	95	372	12.8
2	312	11	97	365	12.8
3	291	21	91	360	12.4
4	332	12	96	375	11.5
5	336	10	98	306	14.2
Average	*310 ± 20*	*13 ± 4*	*95 ± 3*	*360 ± 30*	*12.7 ± 1.0*

To minimize dead-time and pile-up effects, the maximum count rate was restrained to approximately 1% of the maximum output power by adjusting the neutral density filters to control the attenuation of the emitted light. In all rats, the maximum count rate was approximately 800 kHz, except for Rat 3. The tumor diameter for this rate was roughly double the average size and the maximum count rate was 265 kHz. Upon visual inspection, this tumor had a large necrotic center, which limited the maximum count rate. However, the signal-to-noise ratio of the acquired DCE data was still quite high.

3.2 Optical Properties

Table 2 lists the retrieved optical properties of the tumors obtained by fitting the solution to the diffusion equation for transmittance through an infinite homogenous slab.

Table 2. Measured tumor optical properties by the TR-NIRS system.

Rat	μ_s' (cm^{-1})	μ_a (cm^{-1})
1	17.98	1.07
2	28.03	1.45
3	30.95	1.52
4	21.35	0.99
5	12.08	0.84
Average	*22 ± 8*	*1.2 ± 0.3*

The average optical properties, μ_s' and μ_a, were 22 ± 8 and 1.2 ± 0.3 cm^{-1}, respectively. These values are in reasonable agreement with a previous study: 15 ± 7 and 1.4 ± 0.7 cm^{-1} for μ_s' and μ_a, respectively[14]. Differences between the studies could be partly attributed to the difference in cell lines. Rat colon adenocarcinoma cells were used by Van Hillegersberg et al, while the current study used Lovo human adenocarcinoma cells. Furthermore, measurements by Van Hillegersberg et al. were conducted on ex vivo samples using the integrating sphere technique, compared to in vivo TR-NIRS measurements used in the current study.

3.3 Sample of Measured Concentration Curves

Figure 2 shows an example of arterial and tumor contrast agent concentration curves, which were acquired simultaneously during the passage of an ICG bolus.

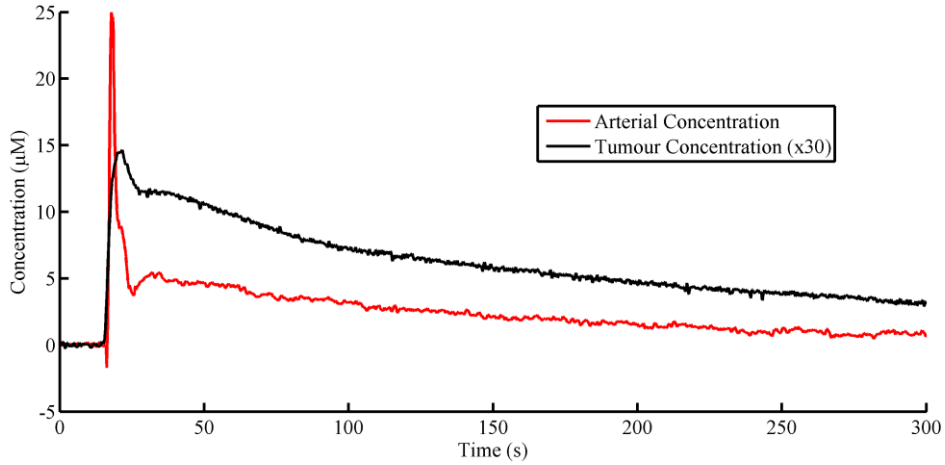

Figure 2. Arterial (red) and tumor (black) contrast agent concentration curves measured by the dye densitometer and TR-NIRS system, respectively, following a bolus injection of ICG.

In comparison, Figure 3 depicts the arterial and tumor contrast agent concentration curves acquired with IRD_{cxb}. In both figures, the distinctive hump occurring approximately at 20 seconds after contrast agent injection reflects the initial passage of the bolus through the interrogated tissue volume and is characteristics of the finite capillary transit time. After the first pass, the tissue concentration curve for ICG mirrors the slow washout of contrast agent from blood. In contrast, the continual rise of the tissue concentration curve for IRD_{cxb} reflects the extraction of the dye into the interstitial space of the tumor. This visible difference in the clearance curves for the two dyes reflects the difference in molecular weight. That is, ICG due to its binding with albumin is too large to penetrate tumor vessel walls.

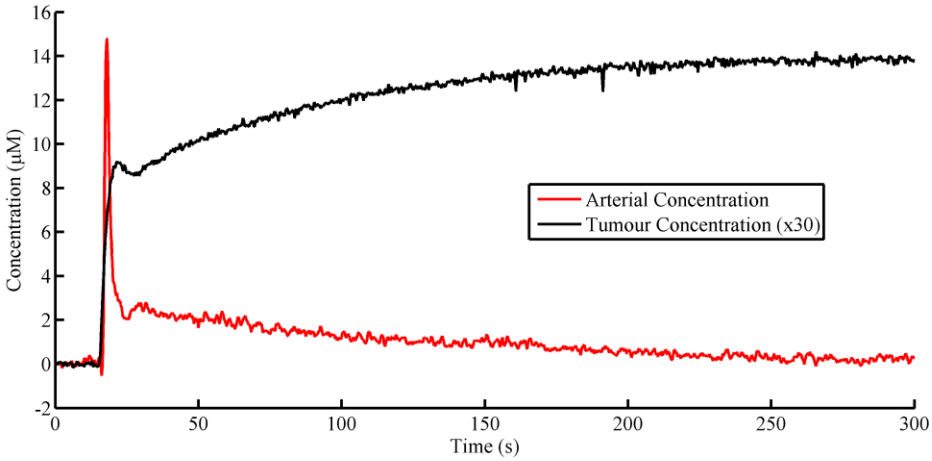

Figure 3. Arterial (red) and tumor (black) contrast agent concentration curves measured by the dye densitometer and TR-NIRS system, respectively, following a bolus injection of IRD_{cxb}.

3.4 Fitted Parameter Data

For each rat there were two injections of each contrast agent, ICG and IRD_{cxb}. Tables 3 and 4 list the fitting parameters for the AATH and VD models when applied to ICG data, respectively. Similarly, Tables 5 and 6 list the fitting parameters for the two models when applied to IRD_{cxb} data. Note, Rat 2 was not included in the ICG results (Tables 3 and 4) because only IRD_{cxb} was injected. All comparisons were conducted by multivariate analysis of variance (MANOVA) run in IBM SPSS Statistics 20 (significant difference was defined as $p<0.05$).

Table 3. Retrieved fitting parameters extracted by the AATH model for ICG clearance data.

Rat	F (ml/g/min)	t_c (s)	E	k_e (min^{-1})	V_c (ml/g)	PS (ml/g/min)
1	0.371	7.0	0.27	2.9	0.043	0.117
3	0.194	12.3	0.33	2.0	0.040	0.078
4	0.177	12.7	0.04	0.2	0.038	0.007
5	0.239	6.8	0.30	3.6	0.027	0.085
Average	*0.25 ± 0.09*	*10 ± 3*	*0.2 ± 0.1*	*2 ± 1*	*0.04 ± 0.01*	*0.07 ± 0.05*

Table 4. Retrieved fitting parameters extracted by the VD model for ICG clearance data.

Rat	F (ml/g/min)	t_c (s)	E	k_e (min^{-1})	α^{-1}	V_c (ml/g)	PS (ml/g/min)
1	0.46	7.8	0.0100	0.154	0.80	0.060	0.0020
3	0.23	14.7	0.0175	0.019	0.65	0.056	0.0018
4	0.22	10.8	0.0240	0.012	0.45	0.040	0.0023
5	0.29	7.6	0.0125	0.005	0.68	0.037	0.0016
Average	*0.3 ± 0.1*	*10 ± 3*	*0.016 ± 0.006*	*0.05 ± 0.07*	*0.6 ± 0.1*	*0.05 ± 0.01*	*0.0019 ± 0.0003*

Comparing the values in Tables 3 and 4, significant differences between the two models for ICG clearance data were observed for E, k_e, and PS (α^{-1} was not used in the MANOVA). In general, the fit of the AATH model was much poorer than the VD model, particularly during the first pass, as illustrated in Figure 4. A consequence of the poor fit is statistically greater E values for the AATH model; however, ICG can be considered a macromolecular contrast agent due to the binding albumin. Therefore, its uptake into the tumor extravascular space is likely going to be small, suggesting that the AATH model overestimates the extraction fraction of ICG. In turn, this error leads to erroneous estimates of the extracted clearance rate (k_e) and the calculated PS product.

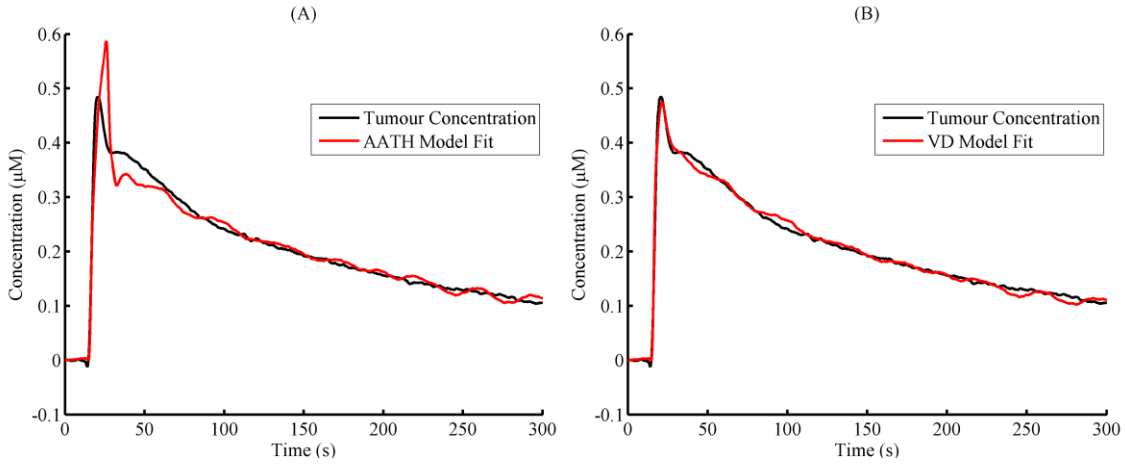

Figure 4. Representative tumor ICG concentration curve (black) and the fit of the (A) the AATH model (red) and (B) the VD model (red).

The fit of the AATH model also appeared worse for the IRD_{cxb} clearance data. However, despite the poorer fit, there were no significant differences observed in any of the fitting parameters listed in Tables 5 and 6 for IRD_{cxb}. This is likely because of differences in the kinetic properties of the two dyes. IRD_{cxb} is considerably smaller than ICG and will likely leak into the extravascular space.

Table 5. Retrieved fitting parameters extracted by the AATH model for IRD_{cxb} clearance data.

Rat	F (ml/g/min)	t_c (s)	E	k_e (min^{-1})	V_c (ml/g)	PS (ml/g/min)
1	0.293	11.0	0.189	0.098	0.054	0.027
2	0.248	15.8	0.346	0.145	0.065	0.046
3	0.226	13.9	0.188	0.154	0.052	0.020
4	0.144	18.1	0.224	0.085	0.043	0.016
5	0.162	8.8	0.161	0.171	0.024	0.012
Average	*0.21 ± 0.06*	*14 ± 4*	*0.22 ± 0.07*	*0.13 ± 0.04*	*0.05 ± 0.02*	*0.02 ± 0.01*

Table 6. Retrieved fitting parameters extracted by the VD model for IRD_{cxb} clearance data

Rat	F (ml/g/min)	t_c (s)	E	k_e (min^{-1})	α^{-1}	V_c (ml/g)	PS (ml/g/min)
1	0.379	9.4	0.129	0.053	0.94	0.059	0.023
2	0.304	15.2	0.247	0.076	1.00	0.077	0.038
3	0.340	10.1	0.110	0.096	0.98	0.057	0.017
4	0.211	12.9	0.132	0.033	0.97	0.045	0.013
5	0.188	8.0	0.129	0.140	0.46	0.025	0.011
Average	*0.28 ± 0.08*	*11 ± 3*	*0.15 ± 0.06*	*0.08 ± 0.04*	*0.9 ± 0.2*	*0.05 ± 0.02*	*0.02 ± 0.01*

Comparing the best-fit parameters from the AATH model between the two contrast agents (Tables 3 and 5), a significant difference was only observed for k_e. However, the variability in some of the other parameters, notably E, was large due to the poor fit of the model. In contrast, significant differences for E and the PS product were found when comparing the best-fit estimates from the VD model (Tables 4 and 6). This result agrees with the expected difference between these contrast agents considering the difference in molecular weight: 67 and 1.17 kDa for ICG and IRD_{cxb}, respectively.

3.5 Mean Difference

Since the VD model demonstrates a better fit, the percent mean difference was determined for each parameter from the two trials (Table 7). The largest variations were observed for E, k_e, and PS for ICG, which is understandable considering the low extraction of this contrast agent. However, a largest variation for k_e was also found for IRG_{cxb}, indicating that this is the least reliable fitting parameter.

Table 7. The relative mean difference (%) between trials for each fitting parameters from the vascular dispersion model applied to clearance data from both contrast agents.

Contrast Agent	ICG (%)	IRD (%)
F	12	30
t_c	14	13
E	84	9
k_e	146	38
α	21	1
V_c	7	13
PS	63	3

4. CONCLUSION

In this work, the ability of two tracer kinetic models, the AATH model and the VD model, to characterize tumor hemodynamics was investigated. The difference between the two models is the original AATH model restricts the capillary transit time t_c to a single value, while the VD model includes an additional parameter to account for the possibility of a distribution of t_c values. The results indicated that this modification improved the tumor concentration curves fitting, particularly for the first pass of the contrast agent. With an appropriate model in base, this approach could be used to characterize the hemodynamic properties of different cancers and their response to treatments. Tumor blood flow and vascular permeability likely play a significant role in the efficacy of therapeutic drugs since they will affect drug delivery. This method could be combined with the quantitative receptor imaging approach proposed by Tichauer et al. to further enhance the characterization of cancer by optical techniques[15].

ACKNOWLEDGMENTS

This work was supported by the Canadian Institutes of Health Research and the National Science and Engineering Council of Canada.

REFERENCES

[1] Astner, S.T., Shi, K., Vaupel, P., and Molls, M., "Imaging of tumor physiology: impacts on clinical radiation oncology.," Experimental oncology 32(3), 149–52 (2010).
[2] Brix, G., Griebel, J., Kiessling, F., and Wenz, F., "Tracer kinetic modelling of tumour angiogenesis based on dynamic contrast-enhanced CT and MRI measurements.," European journal of nuclear medicine and molecular imaging 37 Suppl 1, S30–51 (2010).
[3] Cuccia, D.J., Bevilacqua, F., Durkin, A.J., Merritt, S., Tromberg, B.J., Gulsen, G., Yu, H., Wang, J., and Nalcioglu, O., "In vivo quantification of optical contrast agent dynamics in rat tumors by use of diffuse optical spectroscopy with magnetic resonance imaging coregistration.," Applied optics 42(16), 2940–50 (2003).
[4] Hagen, A., Grosenick, D., Macdonald, R., Rinneberg, H., Burock, S., Warnick, P., Poellinger, A., and Schlag, P.M., "Late-fluorescence mammography assesses tumor capillary permeability and differentiates malignant from benign lesions.," Optics express 17(19), 17016–33 (2009).
[5] Tromberg, B.J., Cerussi, A., Shah, N., Compton, M., Durkin, A., Hsiang, D., Butler, J., and Mehta, R., "Imaging in breast cancer: diffuse optics in breast cancer: detecting tumors in pre-menopausal women and monitoring neoadjuvant chemotherapy.," Breast cancer research : BCR 7(6), 279–85 (2005).
[6] Brown, D.W., Picot, P. a, Naeini, J.G., Springett, R., Delpy, D.T., and Lee, T.-Y., "Quantitative near infrared spectroscopy measurement of cerebral hemodynamics in newborn piglets.," Pediatric research 51(5), 564–70 (2002).
[7] Elliott, J.T., Diop, M., Tichauer, K.M., Lee, T.-Y., and St. Lawrence, K., "Quantitative measurement of cerebral blood flow in a juvenile porcine model by depth-resolved near-infrared spectroscopy.," Journal of biomedical optics 15(3), 037014 (2010).
[8] Diop, M., Tichauer, K.M., Elliott, J.T., Migueis, M., Lee, T.-Y., and St. Lawrence, K., "Comparison of time-resolved and continuous-wave near-infrared techniques for measuring cerebral blood flow in piglets.," Journal of biomedical optics 15(5), 057004 (2010).
[9] Su, M.-Y., Cheung, Y.-C., Fruehauf, J.P., Yu, H., Nalcioglu, O., Mechetner, E., Kyshtoobayeva, A., Chen, S.-C., Hsueh, S., et al., "Correlation of dynamic contrast enhancement MRI parameters with microvessel density and VEGF for assessment of angiogenesis in breast cancer.," Journal of magnetic resonance imaging : JMRI 18(4), 467–77 (2003).
[10] St. Lawrence, K., and Lee, T., "An adiabatic approximation to the tissue homogeneity model for water exchange in the brain: II. Experimental validation.," Journal of cerebral blood flow and metabolism 18(12), 1378–1385 (1998).
[11] Schabel, M.C., "A unified impulse response model for DCE-MRI.," Magnetic resonance in medicine : official journal of the Society of Magnetic Resonance in Medicine / Society of Magnetic Resonance in Medicine 68(5), 1632–46 (2012).

[12] Liebert, A., Wabnitz, H., Grosenick, D., and Macdonald, R., “Fiber dispersion in time domain measurements compromising the accuracy of determination of optical properties of strongly scattering media.,” Journal of Biomedical Optics 8(3), 512–6 (2003).
[13] Contini, D., Martelli, F., and Zaccanti, G., “Photon migration through a turbid slab described by a model based on diffusion approximation. I. Theory.,” Applied optics 36(19), 4587–99 (1997).
[14] Van Hillegersberg, R., Pickering, J.W., Aalders, M., and Beek, J.F., “Optical properties of rat liver and tumor at 633 nm and 1064 nm: photofrin enhances scattering.,” Lasers in surgery and medicine 13(1), 31–9 (1993).
[15] Tichauer, K.M., Samkoe, K.S., Sexton, K.J., Gunn, J.R., Hasan, T., and Pogue, B.W., “Improved tumor contrast achieved by single time point dual-reporter fluorescence imaging.,” Journal of biomedical optics 17(6), 066001 (2012).